Composite Analysis of Long-Lived Mesoscale Vortices over the Middle Reaches of the Yangtze River Valley: Octant Features and Evolution Mechanisms

SHEN-MING FU

International Center for Climate and Environment Sciences, Institute of Atmospheric Physics, Chinese Academy of Sciences, and Institute of Heavy Rain, China Meteorological Administration, Wuhan, China

JING-PING ZHANG

Liaoning Meteorology Bureau, China Meteorological Administration Training Center, Liaoning Branch, Shenyang, China

JIAN-HUA SUN

Laboratory of Cloud–Precipitation Physics and Severe Storms, Institute of Atmospheric Physics, Chinese Academy of Sciences, Beijing, China

TIAN-BAO ZHAO

Key Laboratory of Regional Climate-Environment Research for East Asia, Institute of Atmospheric Physics, Chinese Academy of Sciences, Beijing, China

(Manuscript received 5 March 2015, in final form 2 November 2015)

ABSTRACT

A 14-yr climatology is presented of the mesoscale vortices generated in the vicinity of the Dabie Mountains [Dabie vortices (DBVs)] in the Yangtze River valley. Analyzing these vortices using the Climate Forecast System Reanalysis (CFSR), DBVs were found to be a frequent type of summer mesoscale weather system, with a mean monthly frequency of 12.2. DBVs were mainly located in the middle and lower troposphere, and ~92% of them triggered precipitation. Most DBVs were short lived, and only 19.5% persisted for more than 12 h. Latent heat release associated with precipitation is a dominant factor for the DBV's three-dimensional geometry features, life span, and intensity.

The long-lived DBVs, all of which triggered torrential rainfall, were analyzed using a composite analysis under the normalized polar coordinates. Results indicate that these vortices generally moved eastward and northeastward, which corresponded to the vortices' orientation, divergence, vorticity budget, and kinetic energy budget. The evolution of long-lived DBVs featured significant unevenness: those octants located at the front and on the right side of the vortices' moving tracks were more favorable for their development and maintenance, while those octants located at the back and on the left side acted conversely. Convergence-related shrinking was the most favorable factor for the vortices' development and persistence, while the tilting effect was a dominant factor accounting for their attenuation. Long-lived DBVs featured strong baroclinity, and the baroclinic energy conversion acted as the main energy source for the vortices' evolution. In contrast, the barotropic energy conversion favored the vortices' development and maintenance at first, and later triggered their dissipation.

1. Introduction

For China, heavy rainfall events are the most severe type of weather and have resulted in a large number of disasters (Tao 1980; Zhao et al. 2004). There are three distinct macroregional rainfall characteristics in the areas of northern China, the Yangtze River valley (YRV), and southern China (Tao 1980). Of these three regions, the YRV experiences the most severe precipitation in summer (Zhao et al. 2004; Ding et al. 2007). It has been demonstrated that mesoscale vortices frequently trigger torrential rainfall over the YRV (Tao 1980; Lu 1986; Chen et al. 2003; Zhao et al. 2004; Zhao and Fu 2007; Sun et al. 2010; Fu et al. 2011). In some cases, heavy rainfall associated with the mesoscale vortices can last for several days, causing flash floods, flowing debris, and

Corresponding author address: Shen-Ming Fu, International Center for Climate and Environment Sciences, Institute of Atmospheric Physics, Chinese Academy of Sciences, Huayanli #40, Chaoyang District, Beijing 100029, China.
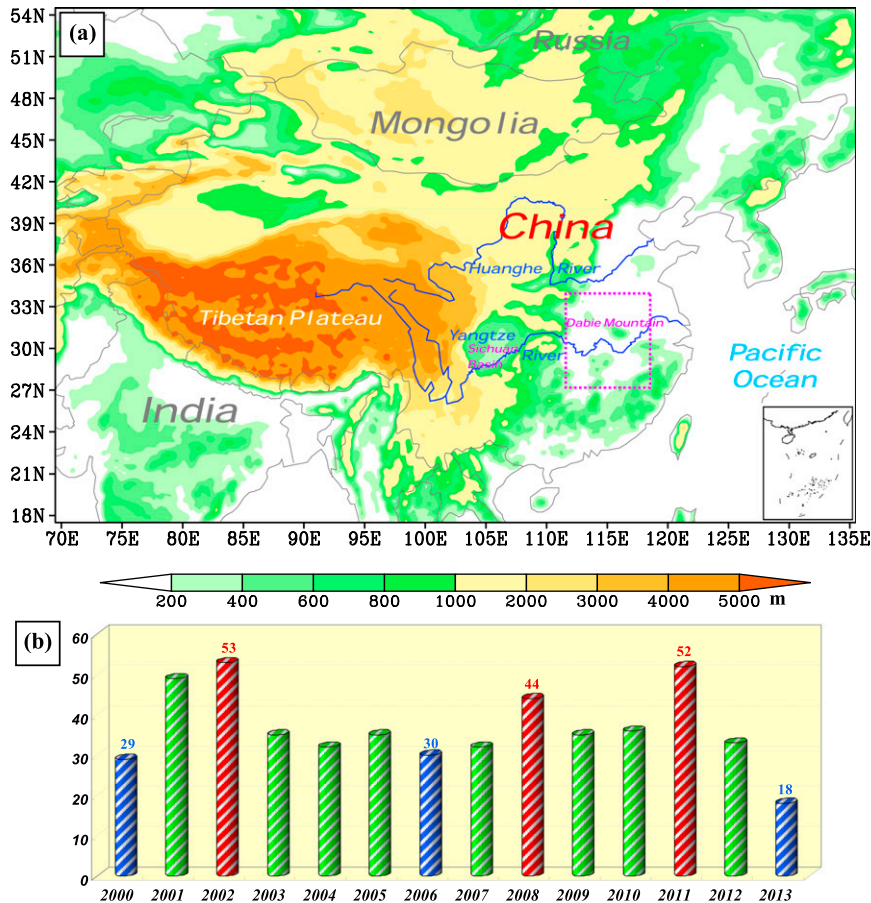E-mail: fusm@mail.iap.ac.cn

FIG. 1. (a) Terrain characteristics (shading, units: m) and the region used for detecting the DBVs. (b) Annual frequency of the DBVs, where red and blue highlight the maximum and minimum annual values respectively.

urban waterlogging that result in substantial casualties and considerable economic loss (Kuo et al. 1988; Fu et al. 2013).

Most of the mesoscale vortices that occur over the YRV mainly originate from two sources (Zhao et al. 2004; Yang et al. 2010; Fu et al. 2013): the Sichuan basin and regions around the Dabie Mountains (Fig. 1a). The mesoscale vortices that initiate from the Sichuan basin are referred to as southwest vortices (Lu 1986; Kuo et al. 1988), and those generating around the Dabie Mountains (Fig. 1a) are defined as Dabie vortices (DBVs) in the present study. Compared to the southwest vortices, which are mainly quasi-stationary within the Sichuan basin (Lu 1986; Fu et al. 2014, 2015), most of the DBVs move rapidly away from their source region (Yang et al. 2010). Extreme DBV cases can persist and cause a series of torrential rainfall events along their tracks that pose a serious flooding threat to the middle and lower reaches of the YRV (Zhao et al. 2004; Fu et al. 2013), where there is dense population and heavy economic development.

As an important torrential rainfall trigger, the DBV has been a topic of considerable research for decades. Typical DBV cases were analyzed in detail, and related studies largely concentrated on DBV synoptic environmental conditions (Gao and Xu 2001; Yang et al. 2010), dynamic/thermodynamic structures (Chen and Dell'Osso 1984; Sun et al. 2010; Zhou and Li 2010), precipitation-related features (Ninomiya 2000; Zhao et al. 2004; Shen et al. 2013), energy conversion characteristics (Fu et al. 2013), and mechanisms accounting for their evolution (Hu and Pan 1996; Dong and Zhao 2004). In contrast, thus far, very few climatological and statistical analyses of DBVs have been conducted. These existing statistical studies (Gu 2008; Yang et al. 2010) have used low-resolution reanalysis data and/or sparse station soundings concentrated on a very short period, and the criteria used for vortex classification were mainly based on large-scale environmental conditions (Yang et al. 2010). Furthermore, so far no efforts have been made to determine the universal or common features of the DBVs'

dynamic and thermodynamic structures, energy conversion processes, and mechanisms that underpin their evolution.

The purpose of this paper is to apply climatological and statistical studies to the DBVs, classify the DBVs based on a new criterion that has significant physical meaning, and conduct composite analyses of the DBVs, thereby determining the universal structural, evolutionary, and energy conversion characteristics of the DBVs.

Data and methods used in this study are described in section 2, statistical and climatological features of the DBVs are presented in section 3, composite analysis results are presented in section 4, and section 5 presents a summary and discussion.

2. Data and methods

a. Data

In this study, we used the National Centers for Environmental Prediction (NCEP) Climate Forecast System Reanalysis (CFSR; Saha et al. 2010) for the summer (June–August) of 2000–13 to detect the DBV, to calculate the dynamic budgets, and to conduct vortex composites. This dataset has a horizontal resolution of $0.5° \times 0.5°$ and a temporal resolution of 6 h. Surface observations every 3 h and soundings every 12 h (0000 and 1200 UTC) from the Chinese Meteorological Administration were used to validate and classify the DBVs detected using the reanalysis. In addition, the precipitation associated with DBVs was investigated by using surface-observed precipitation every 6 h and CMORPH (Climate Prediction Center morphing technique) precipitation data[1] every 3 h (Joyce et al. 2004) from the National Oceanic and Atmospheric Administration (NOAA).

The detection of DBVs was conducted manually using these procedures: 1) at the levels of 950–500 hPa, within the region (27°–34°N, 112°–118°E) (Fig. 1a), when a closed vortex center in the stream field coupled with a significant positive vorticity center was detected for the first time, the initiation of a DBV was defined (Yang et al. 2010); 2) the DBV was considered valid if the observed wind field around the vortex center at three continuous vertical levels also featured significant cyclonic shear; 3) the vertical extent of a DBV was determined by checking all continuous vertical levels for the occurrence of notable vortex circulations at a step of 50 hPa, and the distance between vortex centers in

neighboring vertical levels had to be less than 50 km; 4) at two successive time steps (6 h), the DBV centers at the typical level had to be less than 450 km; and 5) the lifespan of a DBV was defined by the period between the first and last detection of a same vortex.

b. Estimation of DBV size features

To estimate the variation of a DBV's horizontal geometry during different stages and conduct a more effective composite study of the vortices, the size characteristics of a DBV were determined using the method reported by Rudeva and Gulev (2007, 2011) and Fu et al. (2015). Following Fu et al. (2015), the Ertel potential vorticity (PV) (Ertel 1942) was used to estimate the DBV's size; the angular step and the radial spatial step were 10° and 10 km, respectively. The vortex effective radius was defined as $r_{ef} = \sqrt{S_M/\pi}$, where S_M represents the area surrounded by the critical PV value outline M (Fu et al. 2015). This outline M was also used to represent the DBV's horizontal geometry. The maximum and minimum diameters of the outline M were defined as d_{max} and d_{min}, respectively, and the asymmetry of the vortex was defined as d_{max}/d_{min}. At each typical stage, the DBV was normalized to the polar coordinates, and then composite analyses were conducted under this reference frame (Rudeva and Gulev 2007, 2011; Fu et al. 2015). The average of the geometric parameters (r_{ef}, d_{max}, and d_{min}) of the DBVs used in the composite analysis was used to denote the general size features of the corresponding type of DBV. For more detailed information about this method, readers are referred to Rudeva and Gulev (2007, 2011) and Fu et al. (2015).

c. Vorticity and energy conversion budget equations

Because vertical vorticity is an effective measurement of the vortex, a vorticity budget equation was used in this study (Kirk 2003):

$$\frac{\partial \zeta}{\partial t} = \underbrace{-\mathbf{V}_h \cdot \nabla_h \zeta}_{\text{HAV}} - \underbrace{\omega \frac{\partial \zeta}{\partial p}}_{\text{VAV}} + \underbrace{\mathbf{k} \cdot \left(\frac{\partial \mathbf{V}_h}{\partial p} \times \nabla_h \omega \right)}_{\text{TIL}}$$
$$- \underbrace{\beta \upsilon}_{\text{AP}} - \underbrace{(\zeta + f)\nabla_h \cdot \mathbf{V}_h}_{\text{STR}}, \quad (1)$$

where ζ is the vertical vorticity; $\mathbf{V}_h = u\mathbf{i} + \upsilon\mathbf{j}$ is the horizontal velocity vector and $\mathbf{i}$, $\mathbf{j}$, and $\mathbf{k}$ stand for the unit vector points to the east, north, and zenith, respectively; $\nabla_h = (\partial/\partial x)\mathbf{i} + (\partial/\partial y)\mathbf{j}$ is the horizontal gradient operator; f is the Coriolis parameter; p is the pressure; and $\omega = dp/dt$ and $\beta = \partial f/\partial y$. In this study, since the term AP (advection of planetary vorticity) was much smaller than

---

[1] The precipitation of the vortex was first evaluated by using surface-observed precipitation, and when the vortex moved to the sea or other regions without sufficient precipitation observations, CMORPH precipitation data were used in the evaluation.

TABLE 1. Statistical results for the DBVs that lasted more than 12 h: the number and percentage of each type of DBV (NAP), the average life span (ALS), the average maximum 6-h precipitation (AMP), the probability of triggering rainfall (PTR), the mean uppermost stretching level (MUS), the mean lowermost stretching level (MLS), and the mean vertical stretching (MVS).

	NN	PN	NL	PL	Total
NAP (%)	11 (11%)	39 (39%)	7 (7%)	43 (43%)	100 (100%)
ALS (h)	19.6	36.3	18	41.7	35.8
AMP (mm)	16.7	62.5	29.5	69.5	58.8
PTR (%)	54.5%	95%	100%	100%	92%
MUS (hPa)	631	634	665	616	633
MLS (hPa)	905	924	885	940	926
MVS (hPa)	274	290	220	324	293

other terms, only the horizontal advection of vorticity (HAV), vertical advection of vorticity (VAV), titling (TIL), and stretching effects (STR) were analyzed in detail. However, the total effect term (TOT) is defined as TOT = HAV + VAV + TIL + AP + STR.

Since the rotational wind kinetic energy (KE) can represent the intensity of a vortex effectively, budget equations of the rotational wind KE and divergent wind KE (Chen and Wiin-Nielsen 1976; Buechler and Fuelberg, 1986; Fu et al. 2011) were utilized in this study:

$$\frac{\partial K_\psi}{\partial t} = B_\psi + H(K_\chi, K_\psi) + F_\psi, \qquad (2)$$

$$\frac{\partial K_\chi}{\partial t} = B_\chi + H(P, K_\chi) - H(K_\chi, K_\psi) + F_\chi, \qquad (3)$$

$$\frac{\partial (P + I)}{\partial t} = B_{P+I} - H(P, K_\chi) + Q_{P+I} + F_{p+I}, \qquad (4)$$

where K_ψ and K_χ are the rotational wind KE and divergent wind KE; P is the potential energy and I is the internal energy; and ψ and χ denote the stream and potential function, respectively; B_ψ, B_χ, and B_{P+I} stand for the boundary fluxes; F_ψ, F_χ, and F_{p+I} represent the residual terms; and Q_{P+I} denotes the diabatic production/extinction. The term $H(K_\chi, K_\psi)$ is the barotropic energy conversion (BTC), that is, the conversion between the rotational wind KE and the divergent wind KE. The term $H(P, K_\chi)$ is the baroclinic energy conversion (BCC), that is, the transition between the available potential energy (APE) and the divergent wind KE. In this study, the rotational and divergent wind were calculated using the method reported by Cao and Xu (2011) that is effective and accurate in computing the streamfunction and velocity potential of a limited domain.

3. Overview of the statistical and climatological results of the DBVs

During the summers of 2000–13, 513 DBVs were detected (Fig. 1b), with a mean frequency of 12.2 per month, implying that DBVs are very frequent in summer over the YRV. DBVs generally occur most frequently in June (239) and least in August (126). There were three peaks in the annual frequency of DBVs: 2002, 2008, and 2011 (Fig. 1b). The maximum was 53 in 2002 and the minimum was 18 in 2013. In addition, the annual frequency of DBVs had no significant increasing or decreasing trend.

Most DBVs were short-lived, and only 100 (19.5%) lasted for more than 12 h. We classified these 100 DBVs based on the observed surface pressure and precipitation. Following James and Johnson (2010) and Fu et al. (2015), both thermodynamic and dynamic standards were used in the vortex classification, with the respective criteria of whether obvious precipitation occurred (6-h accumulated precipitation ≥ 5 mm) and whether a closed surface low center appeared within 6 h before the initiation of a DBV. As a result, four types of DBVs could be determined: precipitation and surface low (PL), precipitation only (PN), surface low only (NL), and no precipitation and no surface low (NN).

Table 1 shows the statistical characteristics of all four types of DBVs; PL-DBVs account for the maximum fraction (43%) while NL-DBVs were the least common type of event (7%). The PN- and PL-DBVs were much longer lived than the other two types, implying that the latent heat release associated with precipitation may be a necessary condition for the longevity of a DBV. Of the 100 DBVs that persisted for more than 12 h, 92% triggered rainfall during their lifetimes, and the maximum 6-h precipitation amounts of the PL- and PN-DBVs were much larger than for the other two types. All PL- and NL-DBVs triggered rainfall, whereas only about one-half of the NN-DBVs caused precipitation within their lifetimes (Table 1). DBVs were mainly located in the middle and lower troposphere. The greatest vertical extent of these vortices was found to be associated with the PL-DBV category, with a thickness of 324 hPa. In contrast, the NL-DBV was associated with the most limited vertical extent (220 hPa). Only 21 DBV cases lasted for more than 42 h (21%), including 11 PL-DBVs and 10 PN-DBVs,
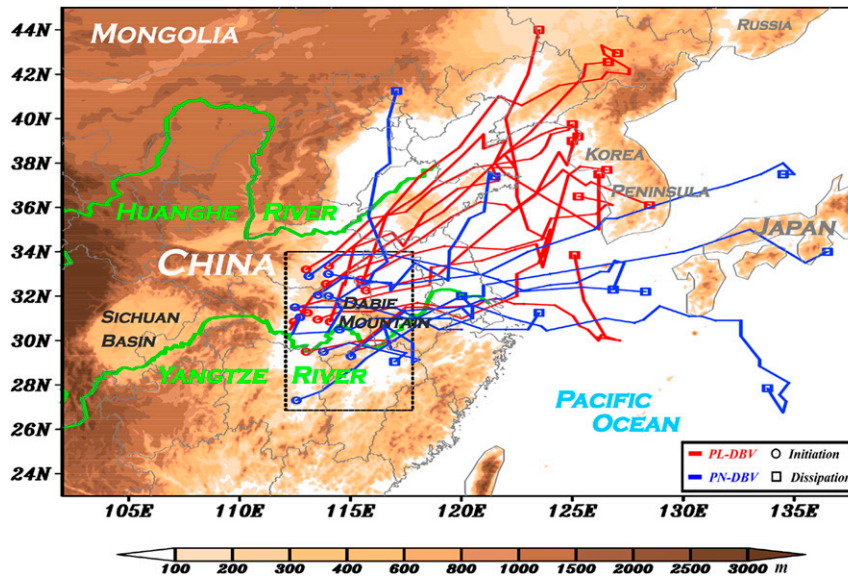
FIG. 2. The tracks of the long-lived DBVs (blue and red solid lines, with circles representing the initiation of the vortex and the rectangles representing the dissipation) and the terrain characteristics (shading, units: m), where the black dashed rectangle denotes the region for detecting the DBVs.

whereas all NL- and NN-DBVs were generally short lived (Table 1). As previous studies have shown (Hu and Pan 1996; Zhao et al. 2004; Yang et al. 2010; Fu et al. 2013), a DBV with a life span of no less than 42 h can be regarded as long lived; therefore, 42 h was used as the threshold value for longevity in the present study. Importantly, all of the 21 long-lived DBVs triggered heavy rainfall, and some caused flash floods and urban waterlogging over the YRV that caused considerable economic loss. Therefore, special attention should be paid to these long-lived DBVs.

The individual tracks of the long-lived DBVs are shown in Fig. 2, which reveals that despite long life cycles these events were generally fast-moving. These vortices can move to northeastern China, the Korean Peninsula, and even Japan, thereby influencing an extremely wide region. The PL-DBVs generally moved northeastward, whereas the PN-DBVs mainly moved eastward (except for one specific case, which, unusually, moved northward).

To facilitate a simple but representative analysis of the DBVs, three typical stages were defined following Fu et al. (2015): the developing stage (DVS), which was the time average of the DBV's formation and 6 h later; the maintaining stage (MTS), which was the time mean of the consecutive 12 h during the midlifetime of the vortex (this is the maximum period during the vortex's maintenance that can be used for all long-lived DBV cases); and the decaying stage (DCS), which was the time average of the DBV's dissipation and 6 h before.

This stage classification ensured that the data of each vortex used in the composition have the same weight, and their effectiveness has been confirmed in analyzing the southwest vortices (Fu et al. 2015).

The mean vertical extent of long-lived DBVs is shown in Table 2. The long-lived DBVs were mainly located in the middle and lower troposphere, with mean thickness maximized in the MTS (325 hPa). The mean central level of long-lived DBVs stretched upward and reached the greatest vertical extent during the MTS, and then the central level moved downward and reached the lowest level of 837.5 hPa in the DCS. In this study, 850 hPa was selected as the typical level for the composite analyses of the long-lived DBVs. This was because 1) 812.5 hPa is the mean central level for these vortices (Table 2), which is the closest commonly analyzed synoptic level of 850 hPa for these events; 2) 850 hPa was very close to the mean maximum vorticity level of the long-lived DBVs (not shown); and 3) 850 hPa has been widely used in case studies of DBVs (Hu and Pan 1996; Fu et al. 2013).

TABLE 2. Mean vertical extent and thickness of the long-lived DBVs during typical stages.

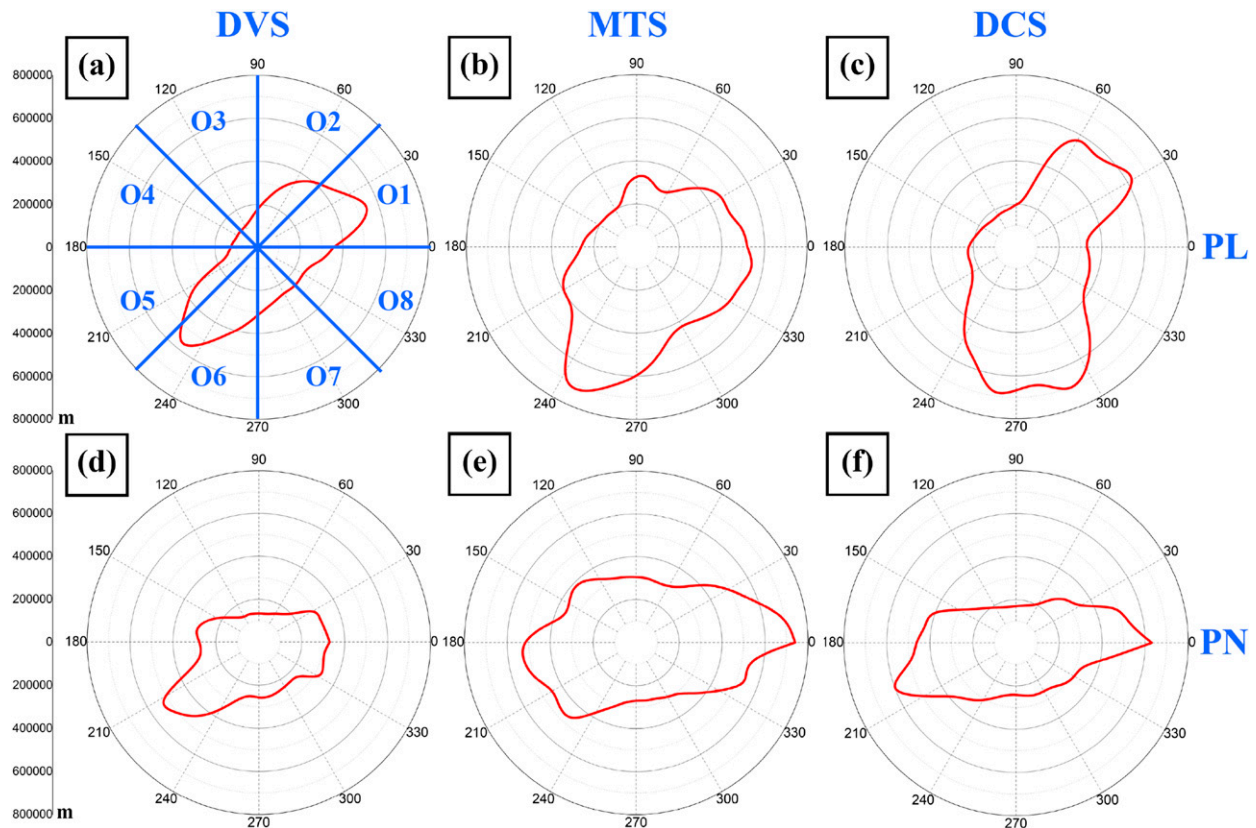| Long-lived DBVs	DVS	MTS	DCS	Entire lifetime
Mean upper level (hPa)	725	625	750	700
Mean lower level (hPa)	900	950	925	925
Mean central level (hPa)	812.5	787.5	837.5	812.5
Mean thickness (hPa)	175	325	175	225

FIG. 3 (a)–(c) The outlines (red solid lines) of the precipitation and surface low (PL) type of DBV during the developing stage (DVS), maintaining stage (MTS), and decaying stage (DCS), respectively, where the blue lines in (a) mark the eight octants (O1–O8) for analysis. (d)–(f) As in (a)–(c), but for the precipitation only (PN) type of DBV.

4. Composite results of long-lived DBVs

a. Mean geometric characteristics of long-lived DBVs

An outline curve (i.e., the closed curve M) of a DBV can be determined using the method reported by Fu et al. (2015). The mean outlines of the long-lived PL- and PN-DBVs are illustrated in Fig. 3. This suggests that the PL-DBVs were mainly oriented southwest–northeast (Figs. 3a–c), which was consistent with the PL-DBVs' main tracks (Fig. 2); however, the PN-DBVs were mainly oriented west–east (Figs. 3d–f), and this was also consistent with their primary track (Fig. 2).

Mean geometric parameters of the long-lived DBVs are shown in Table 3. As illustrated, the DBVs belonged to a type of meso-α weather system (Orlanski 1975; Yang et al. 2010); their mean effective radius minimized during the DVS, maximized in the MTS, and then decreased during the DCS. Generally, the PL-DBVs were larger than the PN-DBVs because both the dynamic and thermodynamic conditions were more favorable during the development of PL-DBVs. The asymmetry of PL-DBVs changed greatly during their lifetimes, with a maximum value of 2.86 appearing in the DVS and a

minimum value of 1.67 appearing during the MTS. In contrast, the asymmetry of the PN-DBVs increased moderately and reached its maximum in the DCS. Overall, the PN-DBVs featured larger asymmetry, except for the DVS.

b. Horizontal structural features of the long-lived DBVs

1) VORTICITY AND DIVERGENCE

Figures 4a–f show the characteristics of vorticity and divergence of the composite PL- and PN-DBV, from which it is clear that the distribution of vorticity showed a pattern of concentric circles, and the vorticity became

TABLE 3. The mean effective radius (units: km) and mean asymmetry of the long-lived DBVs during typical stages.

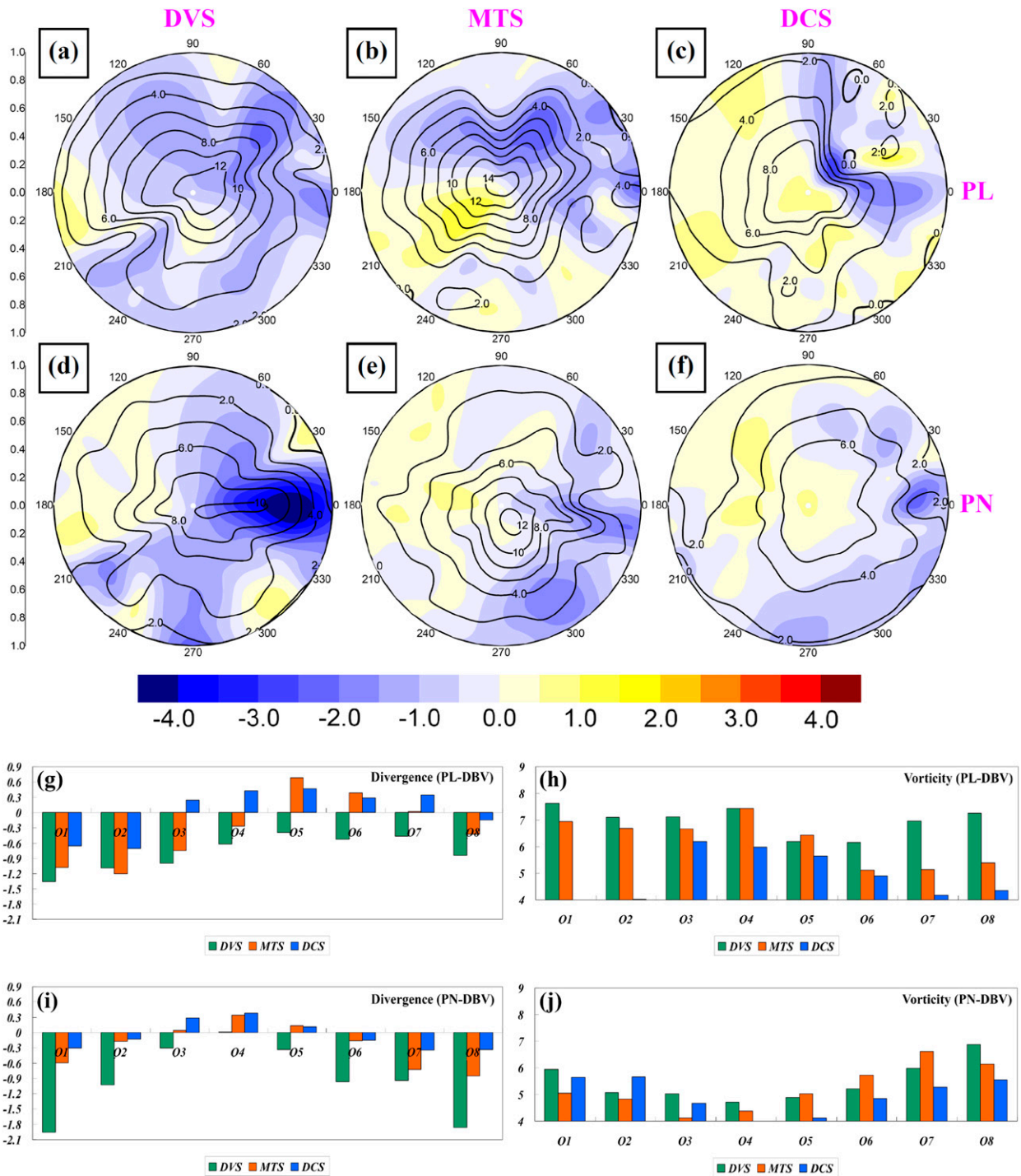|		DVS	MTS	DCS	Entire lifetime
PL-DBV	Effective radius	320	430	428	398
	Asymmetry	2.86	1.67	1.96	2.09
PN-DBV	Effective radius	282	423	351	362
	Asymmetry	2.05	2.11	2.63	2.24

FIG. 4. (a)–(f) The normalized vorticity (black lines, units: $10^{-5}\,\text{s}^{-1}$) and divergence (shading, units: $10^{-5}\,\text{s}^{-1}$) of the composite PL- and PN-DBVs at 850 hPa during the DVS, MTS, and DCS. (g)–(j) The corresponding octant-averaged divergence (units: $10^{-5}\,\text{s}^{-1}$) and vorticity (units: $10^{-5}\,\text{s}^{-1}$).

stronger toward the vortex center. This indicates that the composite results successfully reproduced the main features of the DBVs. Generally, the vorticity of the composite PL-DBV was stronger than that of the PN-DBV

(Table 4), implying that the PL-DBV was of greater intensity. For both types of DBVs, the vortex-mean vorticity maximized during the DVS and minimized in the DCS (Table 4). To investigate detailed features of the

TABLE 4. The vortex-averaged features and budget terms of the composite DBVs during different typical stages, where values not contained within parentheses are the results for the PL-DBVs and the values that are within parentheses are the results for the PN-DBVs.

	DVS	MTS	DCS
Vorticity (10^{-5} s^{-1})	6.9 (5.5)	6.2 (5.2)	4.8 (4.8)
Divergence (10^{-5} s^{-1})	−0.78 (−0.92)	−0.33 (−0.25)	0.04 (−0.06)
Potential temperature (K)	304.1 (302.7)	303.1 (302.3)	301.2 (302.1)
Temperature advection (10^{-5} K s^{-1})	−0.33 (1.54)	0.68 (0.46)	−0.87 (0.64)
Rotational wind KE (J kg^{-1})	20.1 (13.7)	26.8 (21.5)	12.9 (12.4)
Divergent wind KE (J kg^{-1})	0.18 (0.63)	0.29 (0.15)	0.19 (0.09)
Vertical velocity (cm s^{-1})	1.6 (1.4)	1.2 (0.8)	0.6 (0.4)
Specific humidity (g kg^{-1})	12.9 (11.9)	11.9 (11.5)	10.6 (11.3)
TOT (10^{-10} s^{-2})	3.6 (6.8)	3.9 (0.3)	−2.9 (−3.9)
HAV (10^{-10} s^{-2})	−7.1 (−6.1)	−1.6 (−3.2)	1.5 (−0.3)
VAV (10^{-10} s^{-2})	0.4 (4.5)	2.9 (1.8)	0.7 (1.6)
TIL (10^{-10} s^{-2})	−6.2 (−11.1)	−4.6 (−3.4)	−1.8 (−5.8)
STR (10^{-10} s^{-2})	16.4 (19.8)	7.2 (5.2)	−3.3 (0.8)
BCC (10^{-4} W kg^{-1})	13.8 (14.2)	9.1 (4.4)	0.8 (2.5)
BTC (10^{-4} W kg^{-1})	7.9 (10.9)	2.8 (3.4)	−1.5 (−0.3)

vortex, eight octants (O1–O8) were defined, with an angle step of 45° (Fig. 3a).

For the PL-DBV, during the DVS except for O5 and O6, all other octants featured strong positive vorticity (Fig. 4h), indicating that the vortex was of strong intensity. In the MTS, positive vorticity generally weakened (Table 4), whereas vorticity within O1–O5 remained strong. During the DCS, the positive vorticity of the vortex decreased, particularly within O1–O2 and O7–O8, which corresponded to rapid attenuation of the vortex. For the PN-DBV, in the DVS O1 and O7–O8 were characterized by stronger positive vorticity than the other octants (Fig. 4j). During the MTS, the positive vorticity within O6–O8 remained strong, whereas in the DCS, the vorticity within O4–O8 weakened remarkably, corresponding with the dissipation of the vortex.

Divergence associated with both types of DBV was characterized by significant asymmetry (Figs. 4a–f), with strong divergence mainly around the circumference of the vortex. Overall, convergence dominated the DBVs during the DVS and MTS (Table 4), whereas in the DCS, convergence associated with the vortex weakened significantly and divergence dominated some octants of the DBVs (Figs. 4g,i). The PL- and PN-DBV have very different divergence features (Figs. 4a–f): for the PL-DBV, O1–O2 and O8 generally featured convergence throughout the vortex's lifetime (Fig. 4g); however, for the PN-DBV, more octants (O1–O2 and O6–O8) maintained convergence during the whole of the vortex's lifetime (Fig. 4i). Moreover, for both types of DBV, the distribution of divergence was generally consistent with its main moving track (Figs. 2 and 4a–f): strong convergence occurred toward the front of the vortex's moving track and divergence in the wake of the system.

2) KE FEATURES

Rotational wind KE and divergent wind KE of the long-lived DBVs are shown in Fig. 5. This reveals similarities between the PL and PN types of DBVs: 1) the vortex central region generally featured weak rotational wind KE (Figs. 5a–f), whereas the circumference of the vortex mainly featured strong rotational wind KE; 2) O7 and O8 were the advantageous octants, characterized by relatively stronger rotational wind KE throughout the vortices' lifetimes (Figs. 5g,i); and 3) the rotational wind KE maximized during the MTS, but minimized in the DCS (Table 4). On the other hand, the differences between the PL- and PN-DBVs were also significant: 1) for the PN-DBVs, O4 and O5 featured minimum rotational wind KE throughout the vortices' lifetimes, whereas for the PL-DBVs, minimum rotational wind KE appeared within O5–O6 during the DVS and MTS, but in the DCS the minimum appeared within O1–O2 and 2) the rotational wind KE of the PL-DBVs was generally stronger than that of the PN-DBVs (Table 4), indicating that the PL-DBVs were of stronger intensity.

Divergent wind KE was much smaller than the rotational wind KE (Fig. 5, Table 4), and this is consistent with the results of Chen and Wiin-Nielsen (1976). In the DVS, the divergent wind KE of PL-DBV was generally smaller than that of the PN-DBV (Table 4), with the same feature also appearing in the divergence field, whereas the opposite was true during the MTS and DCS. Overall, during the entire lifetime of the vortex, for the PL-DBVs, O2 and O3 featured relatively stronger divergent wind KE (Figs. 5a–c and 5h). For the PN-DBVs, however, O1 and O8 were the relatively stronger octants for the divergent wind KE (Figs. 5d–f and 5j).
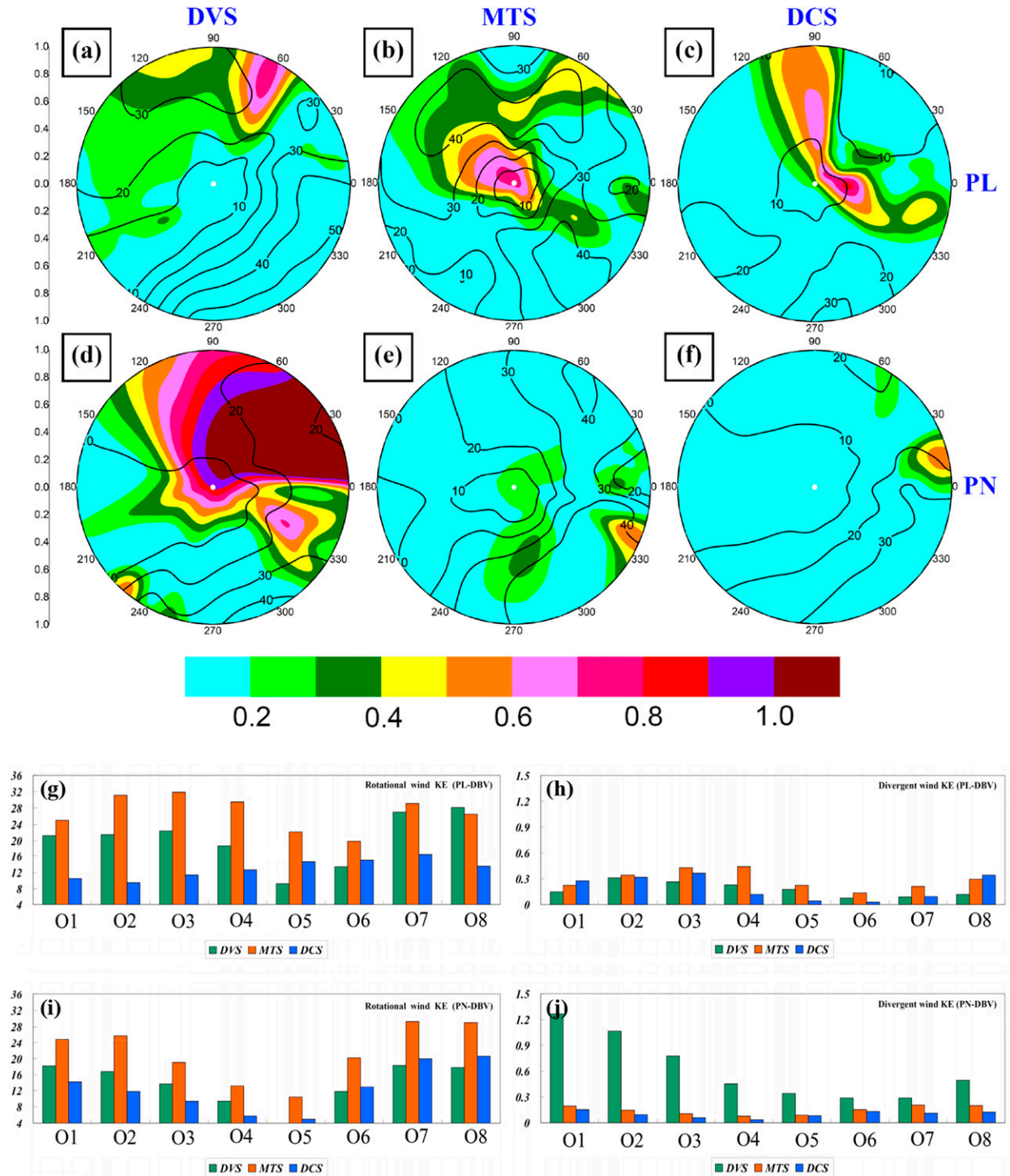
FIG. 5. (a)–(f) The normalized KE of the rotational wind (black lines, units: $J\,kg^{-1}$) and divergent wind (shading, units: $J\,kg^{-1}$) of the composite PL- and PN-DBVs at 850 hPa during the DVS, MTS, and DCS. (g)–(j) The corresponding octant-averaged rotational wind and divergent wind KE (units: $J\,kg^{-1}$).
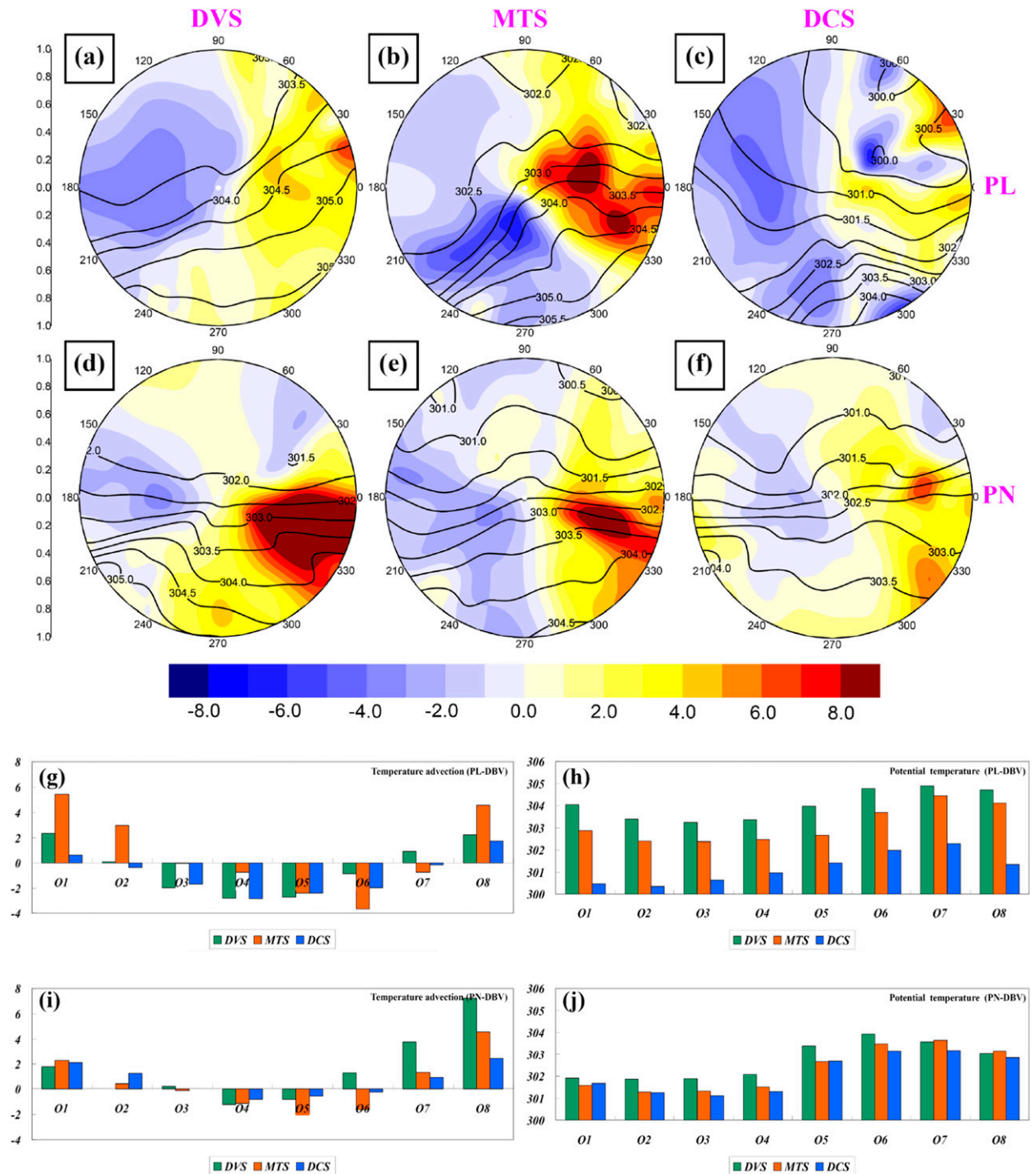
FIG. 6. (a)–(f) The normalized temperature advection (shading, units: $10^{-5}\,\mathrm{K\,s^{-1}}$) and potential temperature (black lines, units: K) of the composite PL- and PN-DBVs at 850 hPa during the DVS, MTS, and DCS. (g)–(j) The corresponding octant-averaged temperature advection (units: $10^{-5}\,\mathrm{K\,s^{-1}}$) and potential temperature (units: K).

3) THERMODYNAMIC STRUCTURES

For both types of DBV, the isentropic lines were dense in the southern part of the vortex (O5–O8), whereas the

northern part generally featured sparse isentropic lines (Figs. 6a–f). This implies that the two types of vortices are characterized by uneven baroclinicity, with the southern part of the vortex stronger than the north. Generally, the

potential temperature decreased to the north (Figs. 6a–f), with O5–O8 warmer than O1–O4 during the entire lifetime of the vortex (Figs. 6h,j). The vortex-averaged potential temperature (Table 4) shows that both types of DBVs became colder during their lifetimes. The PL-DBVs became colder much more rapidly than the PN-DBVs because they were mainly moving north-eastward into a colder ambient environment, whereas the PN-DBVs mainly moved eastward (Fig. 2). In addition, the PL-DBVs were generally warmer than the PN-DBVs, except during the DCS.

For both types of DBVs, temperature advection was strong, which favored the production of APE (Figs. 6a–f). Corresponding with the wind field and the temperature field (not shown), the cold temperature advection mainly appeared in the western octants of the vortex (Figs. 6a–f), whereas the warm advection mainly occurred in the eastern octants. For both the PL- and PN-DBVs, O1 and O8 mainly featured warm temperature advection throughout the vortices' lifetimes (Figs. 6g,i), whereas O4 and O5 were generally dominated by the cold temperature advection.

4) PRECIPITATION-RELATED FEATURES

For both the PL- and PN-DBVs, vortex-averaged specific humidity generally decreased during their lifetime (Table 4), as did the vortex-mean ascending motion, both of which may account for why the maximum 6-h precipitation generally appeared in the DVS and MTS (not shown). Overall, in the DVS and MTS, the vortex-averaged specific humidity and ascending motion were stronger for the PL-DBV (Table 4), which explains why the mean maximum 6-h precipitation associated with the PL-DBV was stronger than that of the PN-DBV (Table 1).

The specific humidity of PL-DBVs mainly decreased northwestward (Figs. 7a–c), whereas the PN-DBVs' specific humidity generally decreased northward (Figs. 7d–f). During the DVS, O1 and O5–O8 of the PL-DBV were characterized by high specific humidity (Fig. 7g), and O5–O8 of the PN-DBV also featured strong specific humidity (Fig. 7i). In the MTS, specific humidity decreased, and strong regions mainly maintained within O1 and O6–O8 of the PL-DBV, as well as O5–O8 of the PN-DBV (Figs. 7g,i). During the DCS, specific humidity of the PL-DBV decreased significantly among all the octants (Fig. 7g), and only O7–O8 featured specific humidity above $11 \, \text{g kg}^{-1}$, whereas for the PN-DBV, although the specific humidity within O5–O8 decreased (Fig. 7i), they were still higher than $11 \, \text{g kg}^{-1}$. In addition, the specific humidity within O1–O3 of the PN-DBV increased. This suggests that, during the DCS, the PN-DBVs were more capable of

producing precipitation, as confirmed by observations (Fig. 8c).

The vertical motions associated with both types of DBVs were generally characterized by remarkable unevenness (Figs. 7a–f), and descending motions mainly occurred around the circumference of the vortex. During the DVS, O1 and O6–O8 of the PL-DBV, as well as O6–O8 of the PN-DBV, featured relatively stronger ascending motion (Figs. 7h,j), and these octants were also characterized by high specific humidity (Figs. 7g,i). This suggests that the conditions within these octants were advantageous to precipitation, which is consistent with observations (Fig. 8a). In the MTS, persistent ascending motion occurs within O1–O2 and O8 of the PL-DBV, as well as O1 and O7–O8 of the PN-DBV, also supporting precipitation (Figs. 7h,j). During the DCS, for both types of DBV, only O1 and O8 featured relatively stronger ascending motion (Figs. 7h,j), and relatively heavier precipitation mainly appeared within O1 and O8 of the PL- and PN-DBV (Fig. 8c).

c. Evolution mechanisms and energy features common among long-lived DBVs

1) VORTICITY BUDGET RESULTS

The distribution of TOT featured remarkable unevenness, which implies that the evolution of DBVs did not take place in a uniform way (Figs. 9a–f). During the DVS, the vortex-mean TOT of both types of DBV was positive (Table 4), indicating that the vortices were in their intensification stage, but the advantageous octants are different for the PL- and PN-DBVs. For the PL-DBVs, positive vorticity within O1–O2 and O7 enhanced rapidly (Figs. 9a,g). The strong positive STR (Figs. 10a,h), which was caused by the intense convergence in these octants (Fig. 4g), dominated the intensification. Overall, STR was the most favorable factor for development of the vortex (Table 4), and VAV only favored intensification slightly; however, TIL and HAV were mainly detrimental for development of the vortex (Figs. 10a,d,g,j; Table 4). In contrast, the advantageous octants (which have larger TOT) for the PN-DBV were O1 and O5–O8 (Fig. 9h). Similarly, the positive STR (Fig. 11h), which was closely related to the significant convergence (Fig. 4i), was the main reason for the PN-DBV's development. In addition, TIL within O7 and VAV within O5–O7 were also favorable (Figs. 11g,i). Overall, STR dominated the PN-DBV's intensification (Table 4; Fig. 11a), and VAV was mainly favorable (Table 4); however, TIL and HAV generally acted in an opposite manner (Table 4; Figs. 11a,d).

In the MTS, TOT of the PL-DBV increased slightly (Table 4), implying that conditions were highly favorable
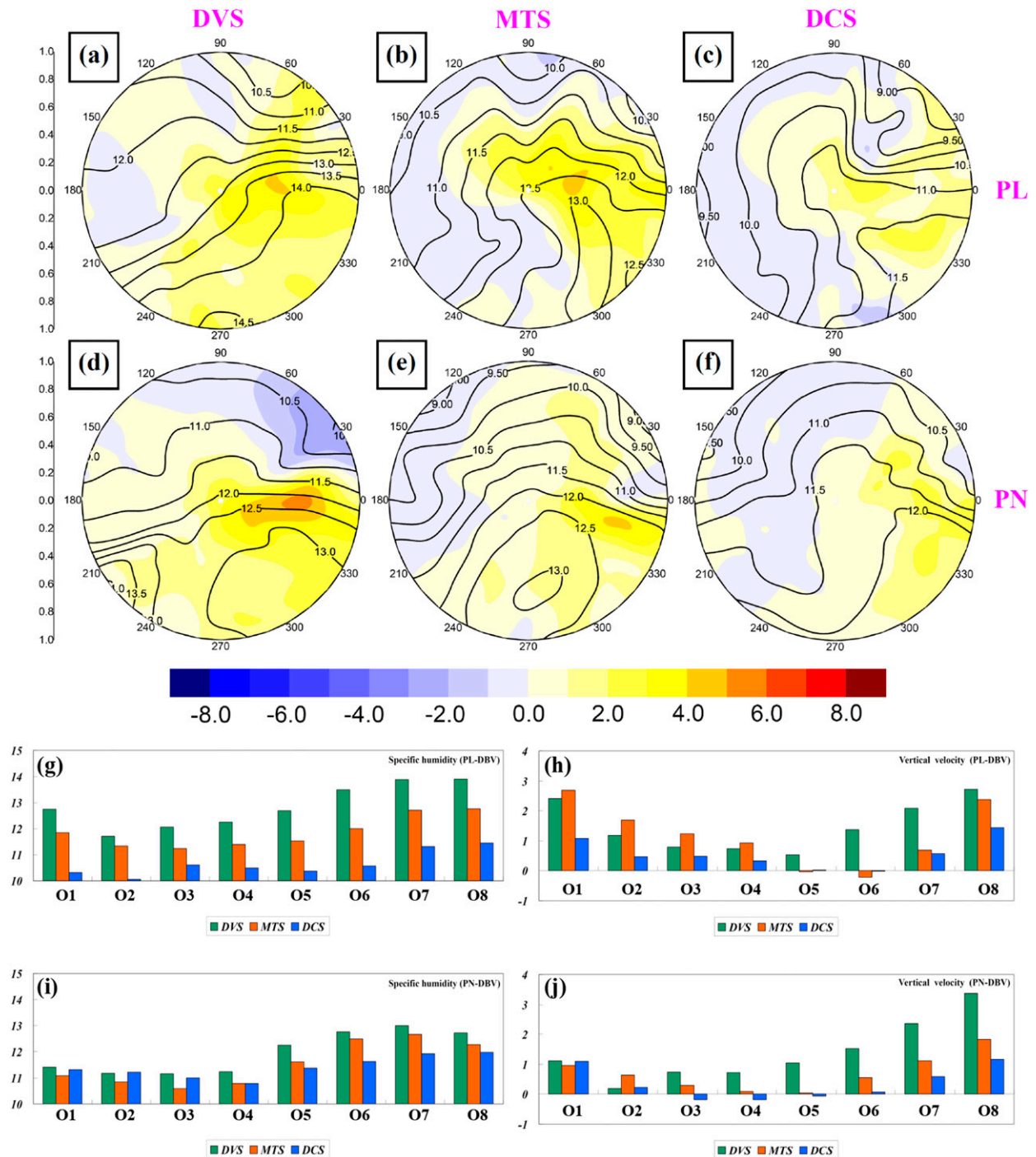
FIG. 7. (a)–(f) The normalized vertical velocity (shading, units: cm s^{-1}) and specific humidity (black lines, units: g kg^{-1}) of the composite PL- and PN-DBVs at 850 hPa during the DVS, MTS, and DCS. (g)–(j) The corresponding octant-averaged vertical velocity (units: cm s^{-1}) and specific humidity (units: g kg^{-1}).

to maintain the vortex. Octants O1–O3 and O8 were characterized by relatively stronger TOT (Fig. 9g), mainly due to the positive STR (Fig. 10h) corresponding to the significant convergence in these octants (Fig. 4g).

In addition, VAV of O1–O2 and O8, as well as HAV within O2–O3 (Figs. 10i,j), also favored maintenance of the vortex. Generally O5–O6 featured rapid attenuation (Fig. 9g). The negative STR (Fig. 10h) associated
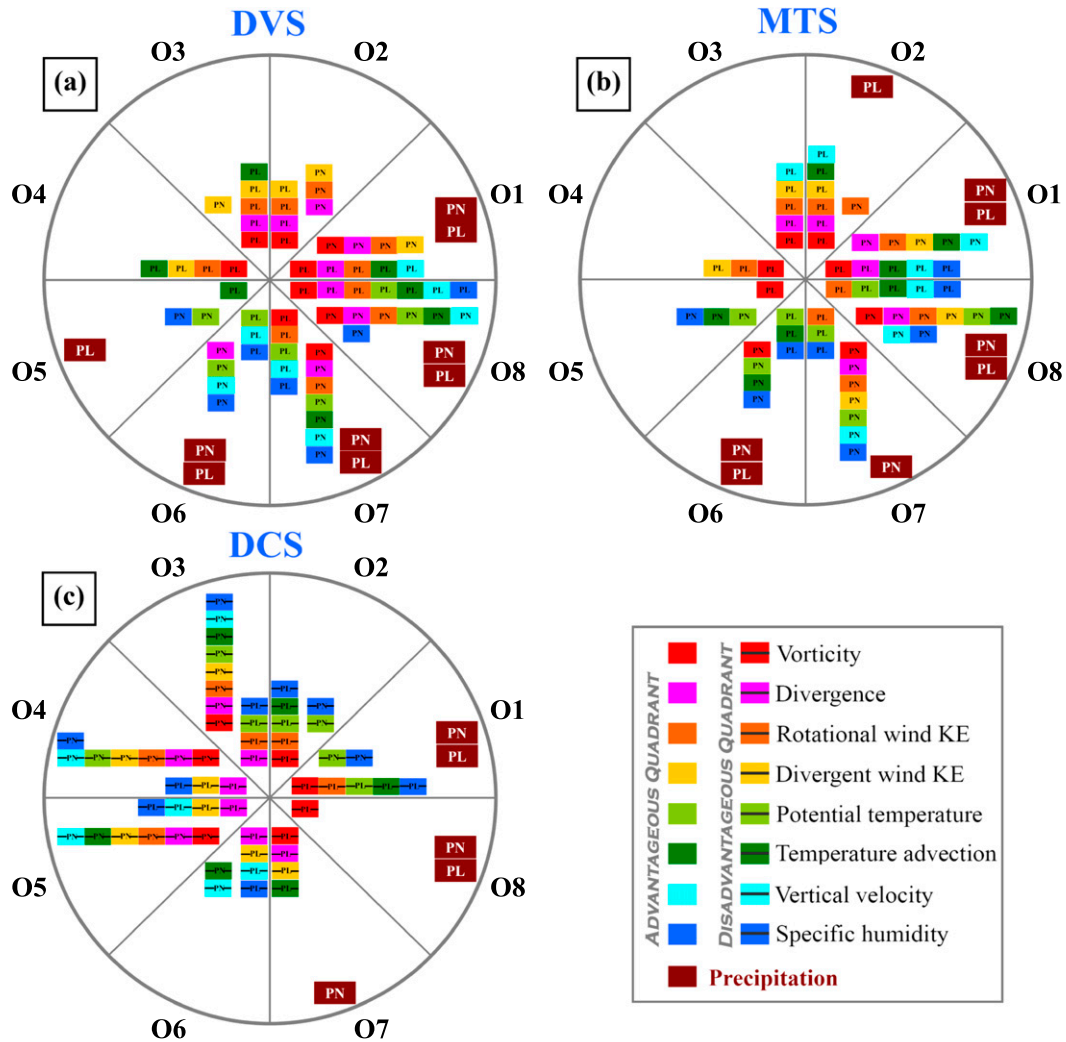
FIG. 8. The favorable and unfavorable octants of the composite PL- and PN-DBVs with respect to their basic features. The octants with significant observed precipitation are also shown. "Favorable" refers to relatively stronger vorticity, convergence, wind KE, potential temperature, temperature advection, ascending motion, and specific humidity; "unfavorable" refers to the opposite.

with divergence (Fig. 4g) and the negative HAV (Fig. 10j) were main mechanisms accounting for the weakening. The configuration of the rapid weakening octants (O5–O6) and the favorable octants (O1–O3 and O8) was generally southwest–northeast (Fig. 9b), which was consistent with the northeastward movement of the PL-DBVs (Fig. 2). Overall, STR and VAV favored the maintenance of PL-DBVs (Table 4), whereas the opposite was true for TIL and HAV. For the PN-DBVs, the vortex-mean TOT was slightly positive (Table 4), implying that the conditions were marginally favorable. Octants O1 and O8 were the most favorable for vortex maintenance (Fig. 9h), mainly due to the positive STR within O1 and O8 (Fig. 11h), as well as the positive VAV of O8 (Fig. 11i). However, O4–O6 were the most detrimental

octants (Fig. 9h). The most detrimental (O4–O6) and the most favorable (O1 and O8) octants were roughly oriented west–east (Fig. 9e), which was in good accordance with the propagation direction of PN-DBVs (Fig. 2). Overall, STR dominated the persistence of PN-DBVs (Table 4) and VAV was also favorable, but HAV and TIL mainly had a negative effect (Figs. 11b,e,g,j; Table 4), which weakened the vortices.

During the DCS, for both types of DBV, TOT became negative (Table 4), which was indicative that the vortices had entered their weakening stage. Overall, TIL and STR dominated the attenuation of PL-DBVs (Table 4), whereas HAV and VAV slowed their dissipation. In contrast, the PN-DBVs weakened in a different way: TIL was the dominant factor for their attenuation (Table 4)
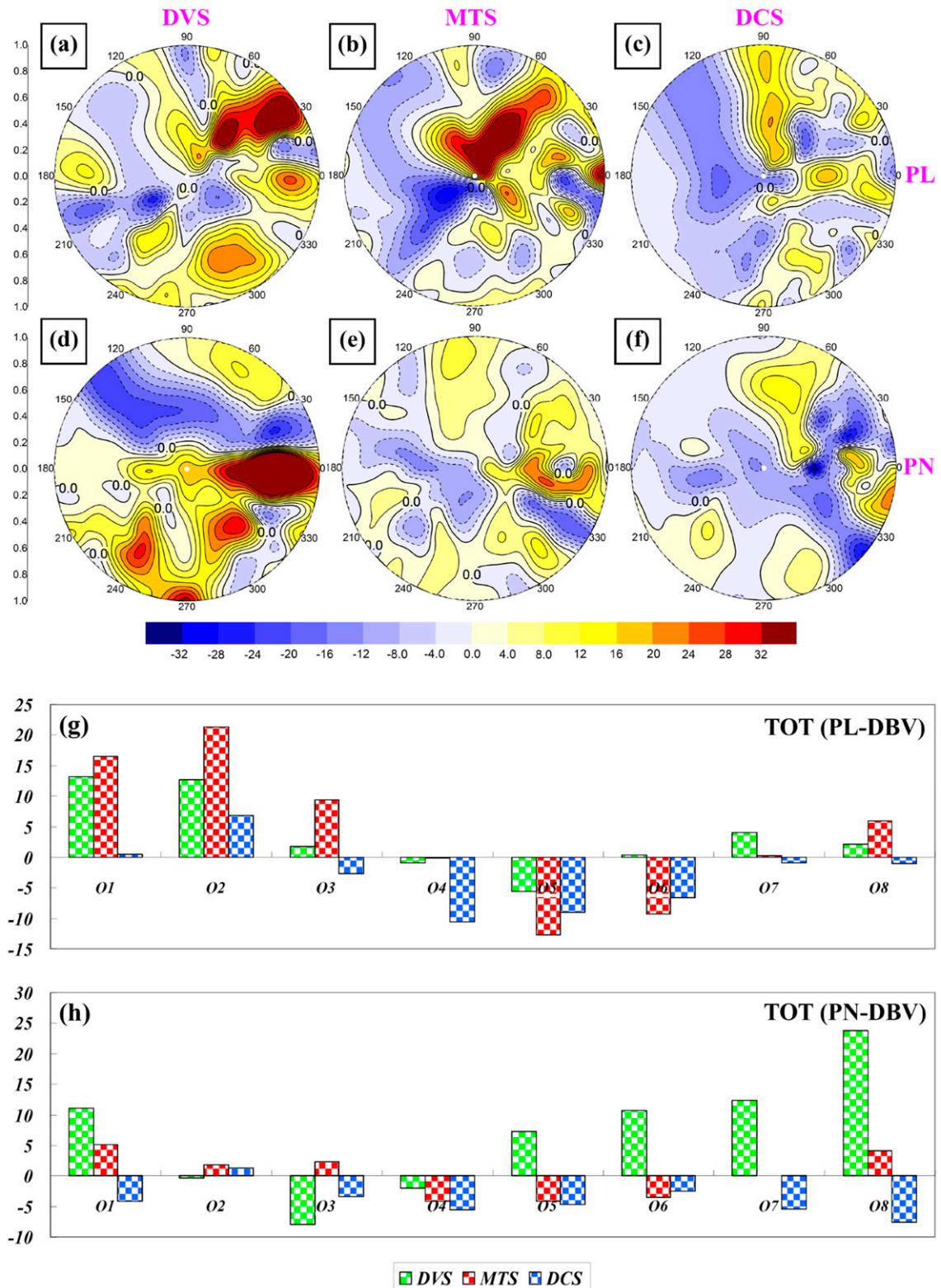
FIG. 9. (a)–(f) The normalized term TOT of the composite PL- and PN-DBVs at 850 hPa during the DVS, MTS, and DCS (units: $10^{-10}\,\mathrm{s}^{-2}$). (g)–(h) The corresponding octant-averaged TOT (units: $10^{-10}\,\mathrm{s}^{-2}$).
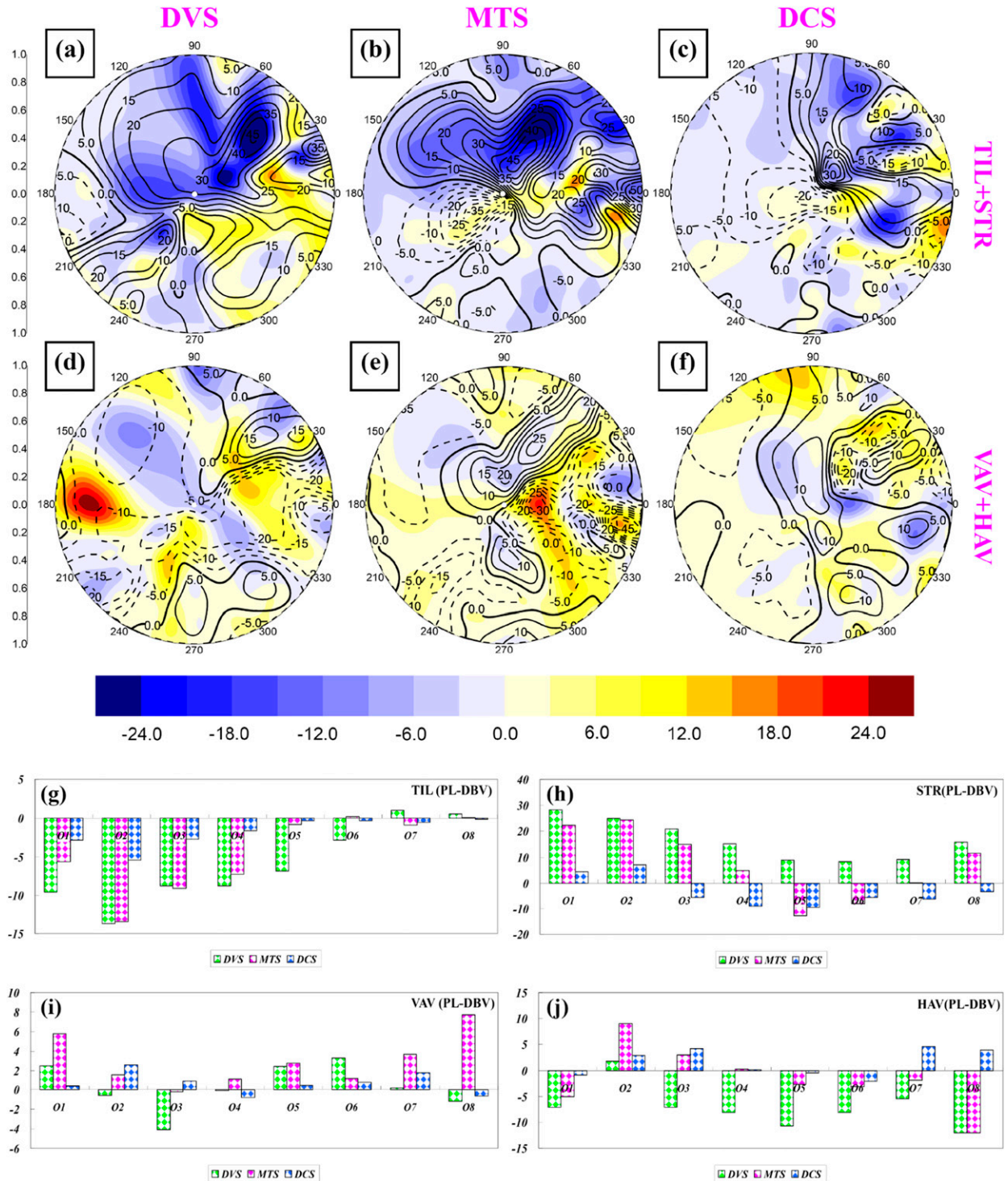
FIG. 10. (a)–(f) The normalized vorticity budget terms of the composite PL-DBVs (units: $10^{-10}\,\mathrm{s}^{-2}$) at 850 hPa during the DVS, MTS, and DCS, where (a)–(c) illustrate TIL (shading) and STR (black lines) and (d)–(f) show VAV (shading) and HAV (black lines). (g)–(j) The corresponding octant-averaged vorticity budget terms (units: $10^{-10}\,\mathrm{s}^{-2}$).
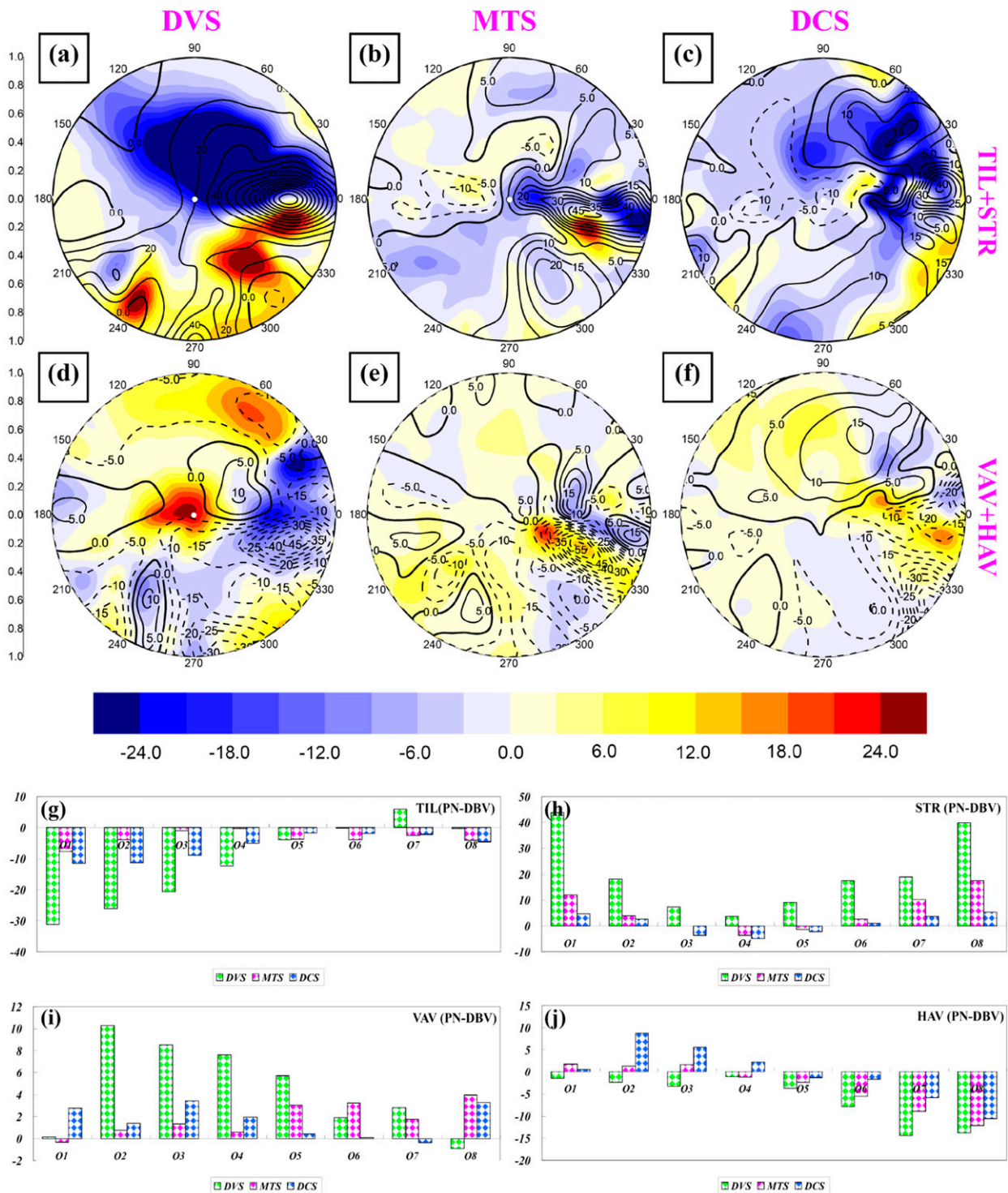
FIG. 11. (a)–(f) The normalized vorticity budget terms of the composite PN-DBVs (units: $10^{-10}\,\mathrm{s}^{-2}$) at 850 hPa during the DVS, MTS, and DCS, where (a)–(c) illustrate TIL (shading) and STR (black lines), and (d)–(f) show VAV (shading) and HAV (black lines). (g)–(j) The corresponding octant-averaged vorticity budget terms (units: $10^{-10}\,\mathrm{s}^{-2}$).

and HAV also accelerated their dissipation, but VAV and STR slowed the decaying process. From Figs. 9c and 9g, O4–O6 of PL-DBVs dissipated much more rapidly than the other octants mainly due to the negative STR (Fig. 10h) associated with divergence (Fig. 4g). For the PN-DBVs, O1, O4–O5, and O7–O8 weakened more rapidly than other octants (Fig. 9h), but the factors accounting for attenuation of these octants were different: TIL dominated the dissipation of O1 (Fig. 11g), TIL and STR dominated the decaying within O4–O5 (Figs. 11g,h), and HAV dominated the attenuation of O7–O8 (Fig. 11j).

2) KE BUDGET RESULTS

The energy conversion processes were closely related to the evolution of the DBVs. As Table 4 shows for both types of DBV, overall BCC maximized in the DVS, which provided sufficient KE for the vortices' development through the release of APE. Then, during the MTS, BCC decreased, implying that the vortices entered a relatively stable stage of maintenance. Finally, during the DCS, BCC reached its minimum, which means that the energy conditions were no longer favorable for the vortices' persistence. Correspondingly, BTC also maximized in the DVS (Table 4), which provided highly favorable energy conditions to enhance the rotational wind KE, and thus the vortices intensified rapidly. Then, during the MTS, BTC weakened significantly, indicating that the vortices had entered a stage of slow variation. Finally, during the DCS, the vortex-mean BTC became negative (Table 4), indicating that the rotational wind KE had converted into divergent wind KE; thus, the vortices dissipated rapidly.

As Fig. 12 illustrates, the energy conversion processes of DBVs were also characterized by asymmetry. Overall, the energy conversion around the circumference of the vortices was stronger than that near their center (Figs. 12a–f), which was generally consistent with distribution of the rotational wind KE (Figs. 5a–f). During the DVS, BCC was strong within O1–O2 and O7–O8 of the PL-DBVs (Figs. 12a,g), whereas strong BTC mainly appeared in O1–O4 (Figs. 12a,h). Therefore, O1 and O2 were highly favorable for the enhancement of PL-DBVs, and TOT also showed the same trend (Fig. 9g). During the MTS, O1–O3 and O8 of PL-DBVs featured strong BCC (Figs. 12b,g), whereas only O2–O3 presented strong BTC (Figs. 12b,h). Therefore, O2–O3 significantly favored PL-DBVs' maintenance, and TOT within O2–O3 was also highly favorable (Fig. 9g). Importantly, the strong negative BCC/BTC region and the intense positive BCC/BTC area (Fig. 12b) were generally oriented southwest–northeast, which was consistent with the main moving tracks of the PL-DBVs (Fig. 2). In the DCS, BCC became negative within O4–O6 of the

PL-DBVs (Figs. 12c,g), and O3–O7 featured relatively stronger negative BTC (Fig. 12h). Thus, the energy conditions of O4–O6 acted to weaken the PL-DBVs rapidly. From Fig. 9g, TOT also indicated that O4–O6 dissipated much more rapidly than the other octants.

For the PN-DBV, there were distinct differences in energy features during its lifetime (Figs. 12a–f). During the DVS, BCC within O1–O2 and O6–O8 featured stronger APE release (Figs. 12d,i), and the BTC of O1–O3 and O7–O8 (Figs. 12d,j) featured stronger energy conversion from the divergent wind KE to the rotational wind KE. Thus, energy conditions within O1–O2 and O7–O8 were highly favorable for rapid intensification of the PN-DBV, and TOT also indicated that O1 and O7–O8 enhanced rapidly (Fig. 9h). During the MTS, O1 and O7–O8 maintained relatively stronger positive BCC and BTC (Figs. 12i,j), implying that energy conversion processes within these octants were generally conducive to the persistence of the vortex. From Fig. 9h, TOT within O1 and O8 also favored the PN-DBV's maintenance. In addition, the relatively stronger negative BCC/BTC octants and the relatively stronger positive BCC/BTC octants (Fig. 12e) were almost oriented west–east, which was in accordance with the predominant tracks of the PN-DBVs (Fig. 2). In the DCS, negative BTC appeared within O2–O6 of the PN-DBV (Figs. 12f,j), which indicates that the rotational wind KE weakened through its conversion to the divergent wind KE. BCC within O3–O7 was very weak (Fig. 12i), implying that the release of APE decreased significantly. Thus, energy conditions within O3–O6 were generally detrimental for maintenance of the vortex, and TOT also indicated that O3–O6 presented a significant weakening trend (Fig. 9h).

5. Summary and discussion

Based on the CFSR reanalysis, climatological and statistical features of the DBVs that generated over the YRV during the summers of 2000–13 were documented. A total of 513 DBVs were detected, with a mean monthly frequency of 12.2, which indicates that DBVs occur very frequently in summer. The monthly frequency of DBVs maximized in June and minimized in August.

The DBVs are mainly located in the middle and lower troposphere. Most of the DBVs were short lived, with only 19.5% persisting for more than 12 h. Of these, 92% triggered rainfall events during their lifetimes. The DBVs that lasted for more than 12 h were classified according to both thermodynamic and dynamic standards (PL, PN, NL, and NN; see section 3 for their definitions). The PL- and PN-DBVs were characterized by much longer life spans, heavier precipitation, and thicker vertical extents than the
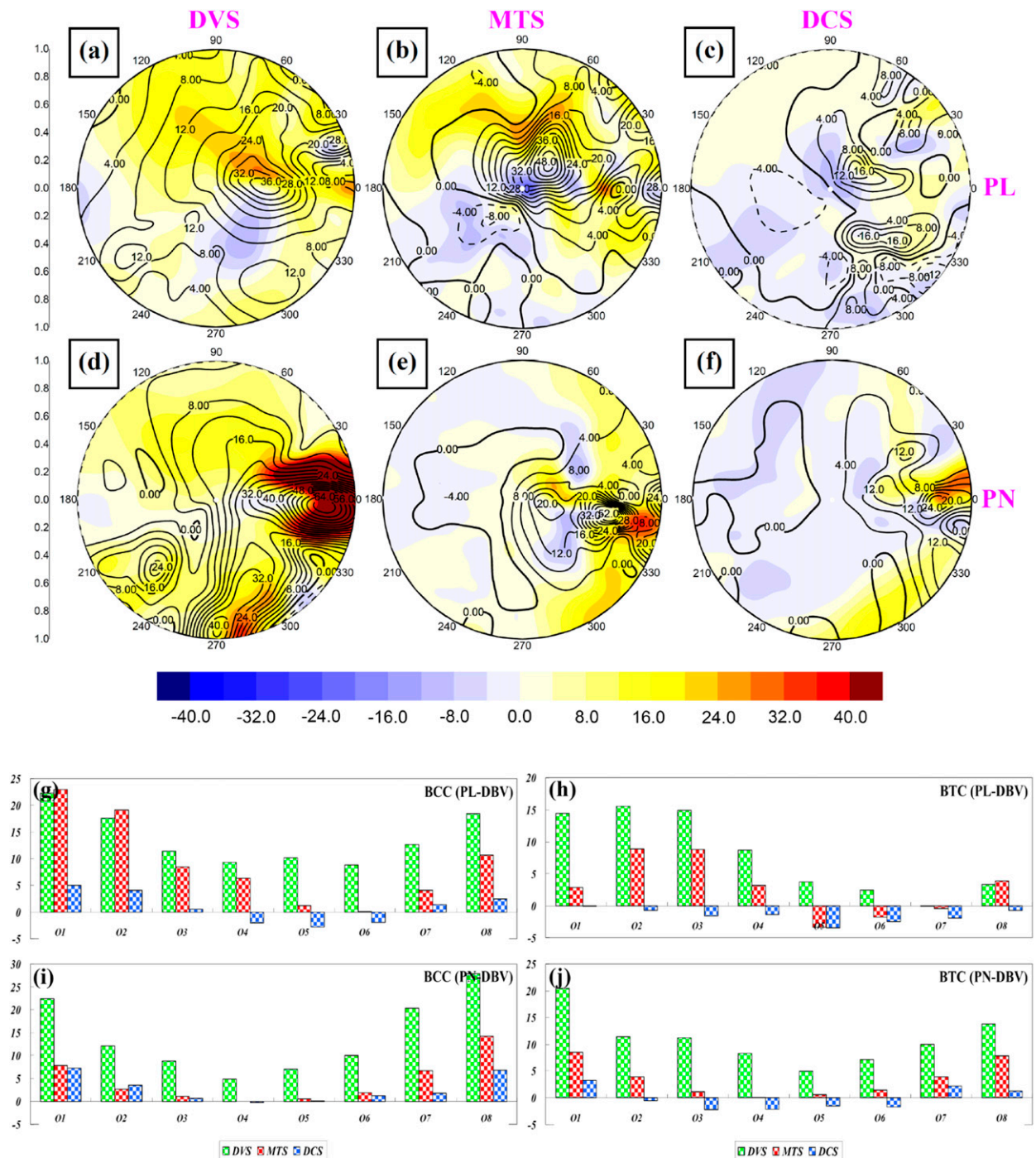
FIG. 12. (a)–(f) The normalized BTC (shading, units: $10^{-4}\,\mathrm{W\,kg^{-1}}$) and BCC (black lines, units: $10^{-4}\,\mathrm{W\,kg^{-1}}$) of the composite PL- and PN-DBVs at 850 hPa during the DVS, MTS, and DCS. (g)–(j) The corresponding octant-averaged BCC and BTC (units: $10^{-4}\,\mathrm{W\,kg^{-1}}$).

other types, implying that latent heat release is vital in determining the characteristics of DBVs.

Based on the statistical results, 21 long-lived DBVs were determined, including 11 PL-DBVs and 10 PN-DBVs, all of which caused torrential precipitation. Generally, the PL-DBVs mainly moved northeastward,

whereas the PN-DBVs mainly moved eastward. Consistent with their preferential tracks, the PL-DBVs generally stretched southwest–northeast, whereas the PN-DBVs were mainly oriented west–east. The PL-DBVs were more intense than the PN-DBVs, with larger effective radii, thicker vertical extents, stronger vorticity and

rotational wind KE, more substantial ascending motion, and heavier maximum precipitation. Both the PL- and PN-DBVs were characterized by significant unevenness, and the baroclinicity within the southern part of the vortex was much stronger than in the northern part. Structural features differed remarkably for the PL- and PN-DBVs, and their main favorable and detrimental octants are summarized in Fig. 8. During the DVS and MTS (Figs. 8a,b), those octants located at the front and on the right side of the vortices' moving tracks (O1–O2 and O7–O8) generally featured many advantageous factors, and thus heavy rainfall was more likely to occur within these octants. In the DCS, the octants located at the back and on the left side of the vortices' tracks (O3–O5) generally featured many unfavorable factors, and thus no heavy rainfall was detected.

The vorticity budget results indicated that octants at the front of the vortices' direction of movement mainly featured favorable conditions for the enhancement of positive vorticity, whereas the opposite was true for the octants at the back. The PL- and PN-DBVs generally developed and persisted in similar ways: during the DVS and MTS, STR associated with convergence was the most favorable factor, and VAV that was closely related to convective activities was also favorable. The opposite was true for TIL and HAV. However, the PL- and PN-DBVs dissipated in very different ways. For the PL-DBVs, the negative STR associated with divergence dominated the attenuation of vortices, and HAV was the main factor acting to resist dissipation, but for the PN-DBVs negative TIL dominated the decaying process, and VAV was the main factor slowing the dissipation.

The energy conversion processes of long-lived DBVs were highly consistent with the vorticity budget results. For both the PL- and PN-DBVs, the release of APE maximized during the DVS, as was the conversion from divergent wind KE to rotational wind KE. Thus, energy conditions were highly favorable for rapid intensification of the vortices. In the MVS, baroclinic energy conversion weakened, particularly for the PN-DBVs. Moreover, the barotropic energy conversion of both types of DBV decreased significantly, implying that the vortices had entered their relatively stable stage of maintenance. During the DCS, the conversion from APE to divergent wind KE decreased significantly and the barotropic energy transition became negative, implying that the rotational wind KE decreased through its conversion to divergent wind KE. Therefore, the energy conditions were no longer favorable for the vortices' persistence, and thus they dissipated rapidly.

The favorable and unfavorable octants in terms of vorticity and KE budgets were summarized in Fig. 13. During the DVS and MTS, those octants located at the front and on the right side of the vortices' moving tracks (O1–O2 and O7–O8) were generally more favorable for their development/maintenance, but for the DCS those octants located at the back and on the left side of the moving tracks (O3–O5) generally dissipated more rapidly. This distribution was highly consistent with the distribution of the basic features shown in Fig. 8.

Fu et al. (2014, 2015) recently conducted statistical and composite studies on the southwest vortices, which is another important type of mesoscale vortices over the YRV. Comparing their results with this study, the mean monthly occurrence (12.2 and 13.8 per month for the DBV and southwest vortex, respectively) and annual occurrence of the DBVs are comparable with those of the southwest vortices. However, the annual frequency differs quite substantially from the southwest vortex climatology. Annual frequency of the DBV had three peaks in 2002, 2008, and 2011. The maximum occurrence of 53 appeared in 2002. In contrast, the southwest vortex only had two peaks in 2001 and 2007, and the maximum occurrence of 55 appeared in 2001. Generally, the DBV is located at lower levels than the southwest vortex, but it covers a much larger horizontal region. DBVs are of greater intensity than southwest vortices, have longer life cycles than southwest vortices, and the DBV can cause heavier rainfall than the southwest vortex. Dynamically, the southwest vortex and DBV develop through similar mechanisms (i.e., positive STR associated convergence), whereas the mechanisms accounting for their persistence and attenuation are very different. The baroclinic energy conversion associated with the DBV is also stronger than that associated with the southwest vortex, and correspondingly, the DBV is also of stronger baroclinity. This result is similar to the mei-yu-front-related studies reported by Kato (1985) and Akiyama (1990).

This paper documents for the first time the universal features of long-lived DBVs, which are vital to understand this type of vortex and the associated heavy rainfall common over the YRV. However, those DBVs that caused torrential rainfall but were short lived should also be investigated in detail, as they were not considered in the present work. Moreover, why the regions around the Dabie Mountains form the source region for the DBVs and what the role is of the Dabie Mountains during the formation stage of the DBVs still remain unclear. We plan to address these knowledge gaps in future work, and thereby contribute to a more holistic understanding of DBVs.
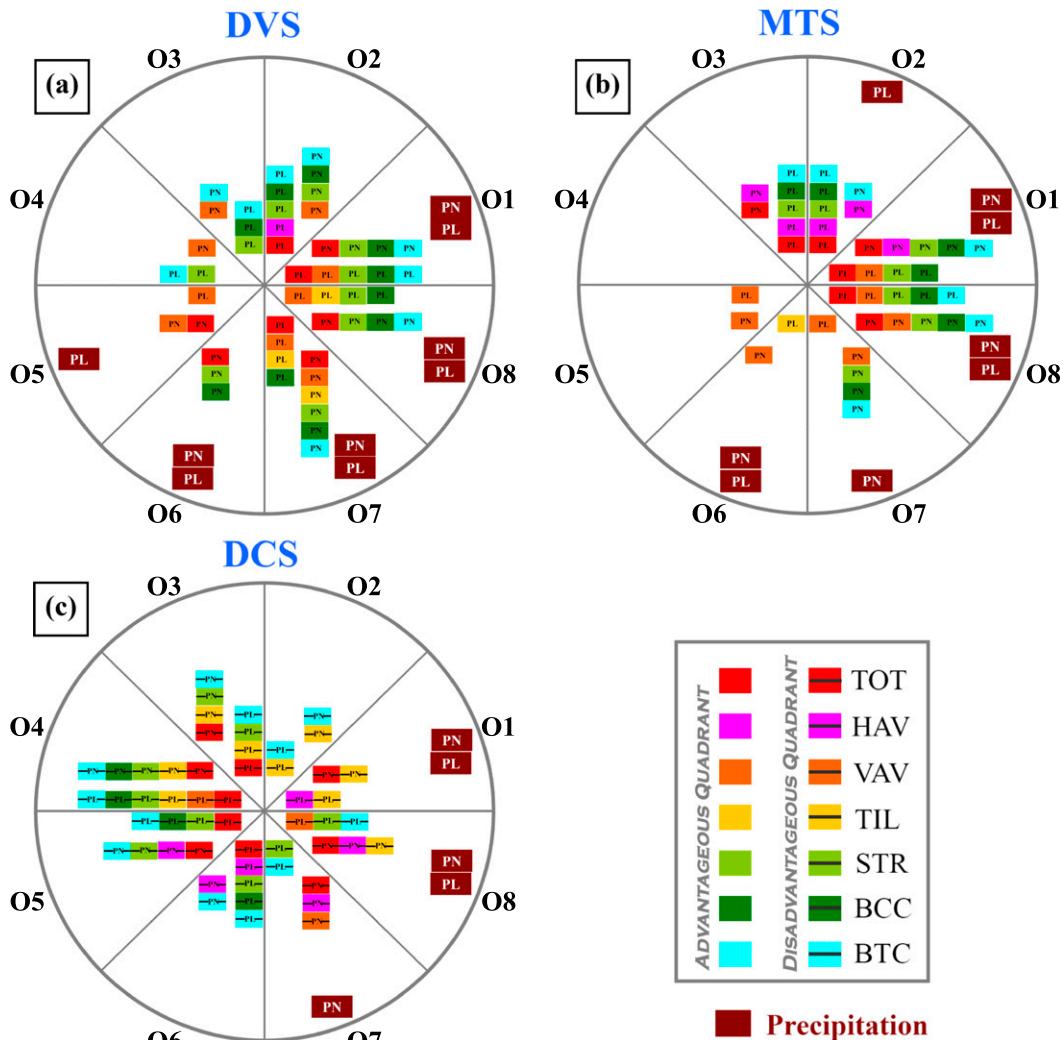
FIG. 13. The favorable and unfavorable octants of the composite PL- and PN-DBVs with respect to the vorticity and KE budgets. The octants with significant observed precipitation are also shown. "Favorable" refers to relatively stronger positive vorticity and KE budget terms, whereas "unfavorable" means relatively stronger negative vorticity and KE budget terms.

REFERENCES

Akiyama, T., 1990: Large synoptic and meso-scale variations of Baiu front during July 1982. Part II: Frontal structure and disturbances. *J. Meteor. Soc. Japan*, **68**, 557–574.

Buechler, D. E., and H. E. Fuelberg, 1986: Budgets of divergent and rotational kinetic energy during two periods of intense convection. *Mon. Wea. Rev.*, **114**, 95–114, doi:10.1175/1520-0493(1986)114<0095:BODARK>2.0.CO;2.

Cao, J., and Q. Xu, 2011: Computing streamfunction and velocity potential in a limited domain of arbitrary shape. Part II: Numerical methods and test experiments. *Adv. Atmos. Sci.*, **28**, 1445–1458, doi:10.1007/s00376-011-0186-5.

Chen, S.-J., and L. Dell'Osso, 1984: Numerical prediction of the heavy rainfall vortex over eastern Asia monsoon region. *J. Meteor. Soc. Japan*, **62**, 730–747.

Chen, T.-C., and A. Wiin-Nielsen, 1976: On the kinetic energy of the divergent and nondivergent flow in the atmosphere. *Tellus*, **28A**, 486–498, doi:10.1111/j.2153-3490.1976.tb00697.x.

Chen, Z.-M., M.-L. Xu, W. B. Min, and Q. Miu, 2003: Relationship between abnormal activities of southwest vortex and heavy rain the upper reach of Yangtze River during summer of 1998 (in Chinese). *Plateau Meteor.*, **22**, 162–167.

Ding, Y.-H., J.-J. Liu, Y. Sun, Y.-J. Liu, J.-H. He, and Y.-F. Song, 2007: A study of the synoptic–climatology of the meiyu system in East Asia (in Chinese). *Chin. J. Atmos. Sci.*, **31**, 1082–1101.

Dong, P.-M., and S.-X. Zhao, 2004: A diagnostic study of mesoscale lows (disturbances) on Meiyu front and associated heavy rainfall (in Chinese). *Chin. J. Atmos. Sci.*, **28**, 876–891.

Ertel, H., 1942: Ein neuer hydrodynamischer Wirbelsatz. *Meteor. Z.*, **59**, 271–281.

Fu, S., J. Sun, S. Zhao, and W. Li, 2011: The energy budget of a southwest vortex with heavy rainfall over South China. *Adv. Atmos. Sci.*, **28**, 709–724, doi:10.1007/s00376-010-0026-z.

——, F. Yu, D. Wang, and R. Xia, 2013: A comparison of two kinds of eastward-moving mesoscale vortices during the mei-yu period of 2010. *Sci. China Earth Sci.*, **56**, 282–300, doi:10.1007/s11430-012-4420-5.

——, J. Zhang, J. Sun, and X. Shen, 2014: A fourteen-year climatology of the southwest vortex in summer. *Atmos. Oceanic Sci. Lett.*, **7**, 510–514, doi:10.3878/AOSL20140047.

——, W. Li, J. Sun, J. Zhang, and Y. Zhang, 2015: Universal evolution mechanisms and energy conversion characteristics of long-lived mesoscale vortices over the Sichuan Basin. *Atmos. Sci. Lett.*, **16**, 127–134, doi:10.1002/asl2.533.

Gao, K., and Y.-M. Xu, 2001: A simulation study of structure of mesovortices along Meiyu front during 22–30 June 1999 (in Chinese). *Chin. J. Atmos. Sci.*, **25**, 740–756.

Gu, W.-L., 2008: The statistical analysis and simulation research of mesoscale vortex along the Meiyu front over the lower reach of Yangtze River in China. M.S. thesis, Nanjing University of Information Science and Technology, 77 pp.

Hu, B.-W., and E.-F. Pan, 1996: Two kinds of cyclonic disturbances and their accompanied heavy rain in the Yangtze River Valley during the Meiyu period (in Chinese). *J. Appl. Meteor. Sci.*, **7**, 138–144.

James, E. P., and R. H. Johnson, 2010: Patterns of precipitation and mesolow evolution in midlatitude mesoscale convective vortices. *Mon. Wea. Rev.*, **138**, 909–931, doi:10.1175/2009MWR3076.1.

Joyce, R. J., J. E. Janowiak, P. A. Arkin, and P.-P. Xie, 2004: CMORPH: A method that produces global precipitation estimates from passive microwave and infrared data at high spatial and temporal resolution. *J. Hydrometeor.*, **5**, 487–503, doi:10.1175/1525-7541(2004)005<0487:CAMTPG>2.0.CO;2.

Kato, K., 1985: On the abrupt change in the structure of the Baiu front over the China continent in late May of 1979. *J. Meteor. Soc. Japan*, **63**, 20–36.

Kirk, J. R., 2003: Comparing the dynamical development of two mesoscale convective vortices. *Mon. Wea. Rev.*, **131**, 862–890, doi:10.1175/1520-0493(2003)131<0862:CTDDOT>2.0.CO;2.

Kuo Y.-H., L.-S. Cheng, and J.-W. Bao, 1988: Numerical simulation of the l981 Sichuan flood. Part I: Evolution of a mesoscale southwest vortex. *Mon. Wea. Rev.*, **116**, 2481–2504, doi:10.1175/1520-0493(1988)116<2481:NSOTSF>2.0.CO;2.

Lu, J.-H., 1986: *Generality of the Southwest Vortex* (in Chinese). China Meteorological Press, 270 pp.

Ninomiya, K., 2000: Large- and meso-α-scale characteristics of meiyu/baiu front associated with intense rainfalls in 1–10 July 1991. *J. Meteor. Soc. Japan*, **78**, 141–157.

Orlanski, I., 1975: A rational subdivision of scales for atmospheric processes. *Bull. Amer. Meteor. Soc.*, **56**, 527–530.

Rudeva, I., and S. K. Gulev, 2007: Climatology of cyclone size characteristics and their changes during the cyclone life cycle. *Mon. Wea. Rev.*, **135**, 2568–2587, doi:10.1175/MWR3420.1.

——, and ——, 2011: Composite analysis of North Atlantic extratropical cyclones in NCEP–NCAR reanalysis data. *Mon. Wea. Rev.*, **139**, 1419–1446, doi:10.1175/2010MWR3294.1.

Saha, S., and Coauthors, 2010: The NCEP Climate Forecast System Reanalysis. *Bull. Amer. Meteor. Soc.*, **91**, 1015–1057, doi:10.1175/2010BAMS3001.1.

Shen, H.-F., G.-Q. Zhai, J.-F. Yin, W.-B. Zhang, and B. Cha, 2013: Feature analysis of mesoscale vortex over lower reaches of Yangtze River during Meiyu period (in Chinese). *Chin. J. Atmos. Sci.*, **37** (4), 923–932.

Sun, J., S. Zhao, G. Xu, and Q. Meng, 2010: Study on a mesoscale convective vortex causing heavy rainfall during the mei-yu season in 2003. *Adv. Atmos. Sci.*, **27**, 1193–1209, doi:10.1007/s00376-009-9156-6.

Tao, S.-Y., 1980. *Rainstorms in China.* Science Press, 225 pp.

Yang, Y.-M., W.-L. Gu, R.-L. Zhao, and J. Liu, 2010: The statistical analysis of low vortex during Meiyu season in the lower reaches of the Yangtze (in Chinese). *J. Appl. Meteor. Sci.*, **21**, 11–18.

Zhao, S.-X., and S.-M. Fu, 2007: An analysis on the southwest vortex and its environment fields during heavy rainfall in eastern Sichuan Province and Chongqing in September 2004 (in Chinese). *Chin. J. Atmos. Sci.*, **31** (6), 1059–1075.

——, and Coauthors, 2004: *Study of the Mechanism of Formation and Development of Heavy Rainfalls on the Meiyu Front in the Yangtze River* (in Chinese). China Meteorological Press, 282 pp.

Zhou, Y.-S., and B. Li, 2010: Structural analyses of vortex causing torrential rain over the Changjiang-Huaihe river basin during 8 and 9 July 2003 (in Chinese). *Chin. J. Atmos. Sci.*, **34**, 629–639.